



## Research article

## Structures and electron affinity energies of polycyclic quinones

Xucheng Wang, Yao Cheng, Yaofeng Yuan, Yongfan Zhang, Wenfeng Wang\*

Key Laboratory of Molecule Synthesis and Function Discovery, Fuzhou University, Fuzhou 350116, China



## HIGHLIGHTS

- The relationship between electron affinity energy and many factors is revealed.
- The close relationship between the electronic structure and the spatial structure is revealed.
- Various interactions such as orbital, electrostatic, and spatial repulsion are exhibited.

## ARTICLE INFO

## Keywords:

Polycyclic quinones  
Electron affinity energy  
Crystal structure  
Calculation

## ABSTRACT

In this study, quinoid structures, semiquinone radical structures, and electron affinity energies (EAEs) of many polycyclic quinones containing heteroatoms (O, B, and F) or heterocycles (pyrrole, imidazole, and pyrazine) were calculated. Quinones with unstable quinoid structures and stable semiquinone radical structures had high EAEs. The main factors of quinoid structural instability were spatial repulsion and antiaromaticity, and the stability factors of the semiquinone radical structure comprised inductive effects, hydrogen bonds, electrostatic interactions, and orbital interactions. Compound **11** had both the antiaromaticity of the quinoid structure and the orbital interactions of the semiquinone radical structure, thus having the highest EAE. The crystal structure of compound **8** was obtained, and it confirmed the reliability of the calculated results of this work.

## 1. Introduction

Polycyclic quinone has a unique structure that makes it suitable for the molecular design of anticancer drugs [1, 2]. This kind of compound has a planar structure that can intercalate the DNA double-helical structure, and therefore is a DNA intercalator with an inhibitor activity of DNA topoisomerase II [3, 4]. In addition, the quinoid structure of polycyclic quinones can capture electrons leaked from the mitochondrial respiratory chain and transfer them to O<sub>2</sub> to produce reactive oxygen species (ROSs) [5], as shown in Scheme 1. Since ROSs can cause DNA breaking [6], polycyclic quinones are also DNA cleavage agents. Although some anticancer drugs with polycyclic quinone structures, such as doxorubicin and mitoxantrone, are limited due to cardiovascular toxicity [7, 8], polycyclic quinones containing heteroatoms still strongly attract the interest of pharmaceutical chemists [9, 10, 11] because ROSs play a crucial role in the intrinsic apoptotic pathway of cancer cells [12, 13]. Figure 1 shows YM155, which is a clinical drug that causes cancer cell genes to become unstable through autophagy-mediated ROS generation [14]. Compounds A and B promote cancer cell mitochondrial dysfunction through ROS generation, followed by apoptosis [15].

Compound C is reported from our early work, and it loses its anticancer activity when its quinoid structure is destroyed. Moreover, its anticancer activity shows a positive correlation with its ROS generation ability [16]. These studies suggest that the ROS generation ability of polycyclic quinone is closely related to the anticancer drug activity.

As shown in Scheme 1, due to the strong ability of O<sub>2</sub> to obtain electrons, the abilities of quinones to generate ROSs depend mainly on their abilities to acquire electrons. These abilities can be measured by the energy released in the reaction in which a quinoid structure obtains an electron to become a semiquinone radical structure (i.e., electron affinity energy (EAE)). To express the EAEs as positive values, in this paper, the EAEs were obtained from the energies of the quinoid structures minus the energies of the semiquinone radical structures. Factors that destabilize a quinoid structure and stabilize a semiquinone radical structure lead to high EAEs. These factors include hydrogen bonds, spatial repulsion, antiaromaticity, inductive effects, conjugation effects, electrostatic interactions, and orbital interactions. In this work, 12 polycyclic quinones containing these factors were chosen to calculate their EAEs, and the relationship between the structure and EAE was studied. In addition, a crystal structure of polycyclic quinone (compound **8**) was obtained and

\* Corresponding author.

E-mail address: [wangwf@fzu.edu.cn](mailto:wangwf@fzu.edu.cn) (W. Wang).<https://doi.org/10.1016/j.heliyon.2022.e10107>

Received 26 March 2022; Received in revised form 9 June 2022; Accepted 25 July 2022

2405-8440/© 2022 The Author(s). Published by Elsevier Ltd. This is an open access article under the CC BY-NC-ND license (<http://creativecommons.org/licenses/by-nc-nd/4.0/>).

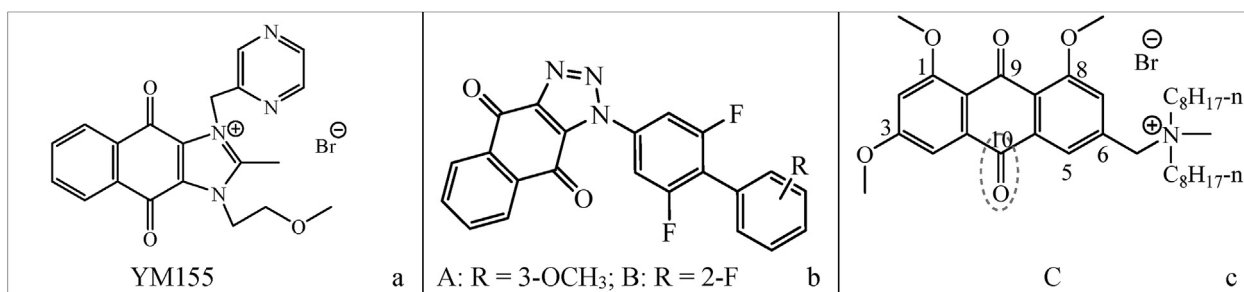
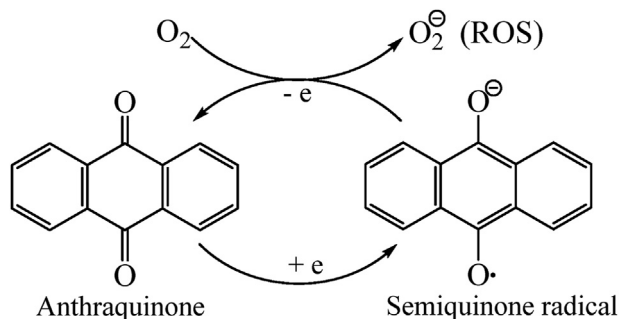


**Figure 1.** Structures of some polycyclic quinones with anticancer activities: (a) clinical drug YM155, (b) reported anticancer agents A and B, and (c) anticancer agent C reported in early work.



**Scheme 1.** Electron transfer mechanism that through which anthraquinone generates reactive oxygen species (ROSs).

compared with the calculated structure, and the result showed that they were very consistent, indicating that the results calculated in this work were reliable.

Although the production of ROSs is a key reason for the anticancer activity of many chemotherapeutic drugs, the ROS generation abilities of chemotherapeutic drugs remain difficult to measure quantitatively. We propose that the EAE is a quantitative measure of the ROS generation ability and discuss the relationship between the molecular structure and EAE. This work can help drug chemists determine what kind of molecular structure can easily generate ROSs, and it provides a reference for anticancer drug design at the molecular level.

## 2. Experiment

### 2.1. Methods and materials

All chemicals and solvents were chemically pure or of analytical purity grade unless otherwise stated. Proton nuclear magnetic resonance ( $^1\text{H}$  NMR) spectra were recorded on a JEOL-500 (500 MHz) and Bruker-

AV (400 MHz) spectrometer with tetramethylsilane (TMS) as an internal standard in dimethyl sulfoxide- $d_6$  (DMSO- $d_6$ ).

#### 2.1.1. Synthesis of compound 8

**2.1.1.1. The synthetic route.** The synthetic route of compound 8 is shown in Scheme 2.

**2.1.1.2. The synthesis of 2,3-diphthalimido-1,4-naphthoquinone.** Potassium phthalidimide (3.26 g, 17.6 mmol) was finely powdered and dried under vacuum then added to a solution of 2,3-dichloro-1,4-naphthoquinone (1 g, 4.4 mmol) in anhydrous acetonitrile (100 mL). The reaction mixture was refluxed for 3h, then the hot solution was filtered. The precipitate was washed successively with cold acetonitrile (100 mL), water (100 mL) and methanol (100 mL). 2,3-Diphthalimido-1,4-naphthoquinone was dried under vacuum at 50 °C and isolated as a pale yellow powder (1.87 g) in 95% yield.

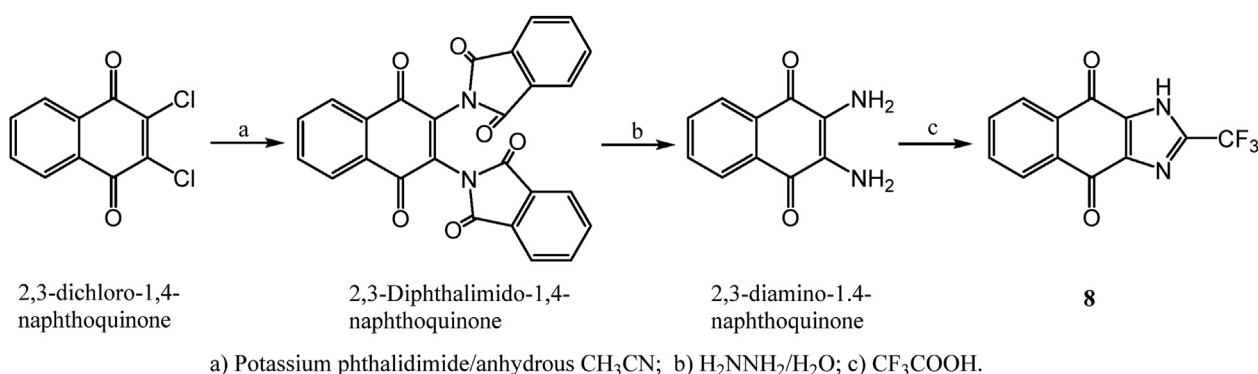
2,3-Diphthalimido-1,4-naphthoquinone is a reported compound [17], here we only list  $^1\text{H}$  NMR date.

$^1\text{H}$  NMR (400 MHz, DMSO)  $\delta$ : 8.21–8.19 (m, 2H, ArH), 8.06–8.04 (m, 2H, ArH), 7.99–7.96 (m, 4H, ArH), 7.95–7.92 (m, 4H, ArH).

**2.1.1.3. The synthesis of 2,3-diamino-1,4-naphthoquinone.** To a suspension of 2,3-diphthalimido-1,4-naphthoquinone (2.24 g, 5 mmol) in water (150 mL) was added an 80% solution in water of hydrazine (16 mL). The solution was stirred for 15 min at room temperature then heated at 65–70 °C for 3h. The reaction mixture was allowed to stand at room temperature. The precipitate was filtered, then washed with a large volume of water. 2,3-Diamino-1,4-naphthoquinone was dried overnight under vacuum at 100 °C and isolated as a purple powder (0.88 g) in 94% yield.

2,3-diamino-1,4-naphthoquinone is a reported compound [17], here we only list  $^1\text{H}$  NMR date.

$^1\text{H}$  NMR (500 MHz, DMSO)  $\delta$ : 7.76 (dd,  $J_1 = 5.6$  Hz,  $J_2 = 3.3$  Hz, 2H, ArH), 7.59 (dd,  $J_1 = 5.6$  Hz,  $J_2 = 3.3$  Hz, 2H, ArH), 5.46 (s, 4H,  $2 \times \text{NH}_2$ ).



**Scheme 2.** The synthetic route of compound 8.

**2.1.1.4. The synthesis of 2-(trifluoromethyl)-1h-naphtho [2,3-d]imidazole-4,9-dione (8).** 2,3-diamino-1,4-naphthoquinone (600 mg, 3.2 mmol) was dissolved in 15 mL trifluoroacetic acid in a 100 mL three-neck flask, then the mixture was stirred at 70 °C for 1h. After the reaction, water (~15 mL) was added into the mixture, then dichloromethane was used to extract the organic phase for three times (3 × 30 mL). The organic phases were combined and dried with anhydrous Na<sub>2</sub>SO<sub>4</sub>, and concentrated under reduced pressure to yield compound **8** without further purification.

2-(trifluoromethyl)-1h-naphtho [2,3-d]imidazole-4,9-dione (**8**) is a reported compound [18], here we only list <sup>1</sup>H NMR data.

<sup>1</sup>H NMR (500 MHz, DMSO) δ: 8.14–8.11 (m, 2H, ArH), 7.90–7.87 (m, 2H, ArH).

## 2.2. Computational method

All the optimized structures were obtained from the full optimization method, and all geometry optimizations and calculations were performed by B3LYP using the Gaussian 09 program with the 6-311+G\*\* basis set for all atoms.

### 2.2.1. Basis set selection

In this work, the cc-PVTZ and 6-311+G\*\* basis sets were both used to calculate the structures of anthracene and phenanthrene, which are polycyclic aromatic hydrocarbons. The calculated results are shown in Figure 2 and Table 1.

As shown in Table 1, the calculated results at the 6-311+G\*\* level and those at the cc-PVTZ level were approximately equal, and they were both close to the experimental results and the calculated results at the cc-PVDZ level. In addition, the difference between the energies of anthracene and phenanthrene was 0.00815 a. u. (21.4 kJ/mol) at the 6-311+G\*\* level and 0.00802 a. u. (21.0 kJ/mol) at the cc-PVTZ level. Based on the enthalpies of formation of anthracene (230.9 kJ/mol) and phenanthrene (207.5 kJ/mol) [23], the energy difference between anthracene and phenanthrene was approximately 23.4 kJ/mol. In summary, both the 6-311+G\*\* basis set and the cc-PVTZ basis set could calculate bond lengths and energies of the polycyclic compound accurately. Since the cc-PVTZ basis set required significantly more calculation time than the 6-311+G\*\* basis set, the latter was chosen to calculate all the compounds studied in this work.

## 3. Results and discussion

### 3.1. Calculations of EAEs

The EAEs of 12 polycyclic quinones were calculated. Their molecular structures and codes are shown in Figure 3, and the calculated results are shown in Table 2.

Among the anthraquinone derivatives (1–4), 1,8-dihydroxyanthraquinone (**2**) and 1,8-dimethoxyanthraquinone (**4**) possessed the largest and smallest EAEs, respectively. The EAEs of the other polycyclic quinones were as follows: 1) in five-membered heterocyclic quinones (5–8), the electron-withdrawing group increased the EAE and the electron-donating group reduced the EAE, while the EAEs of quinones containing imidazole rings (6–8) were significantly higher than that of the pyrrole ring (5). 2) The EAEs of quinones containing six-membered heterocyclic rings (9) increased significantly after oxidation to the corresponding N-oxide (10). 3) The quinone bound to B atoms (11) had the largest EAE, indicating that quinones containing B atoms were good ROS generators.

### 3.2. Polycyclic quinones with oxygen-containing groups

#### 3.2.1. Hydrogen bond and repulsion

The optimized structures of compounds **2** and **4**, as well as their resonance structures, are shown in Figure 4.

Both the semiquinone radicals of compounds **2** and **4** had two resonance structures, as shown in Figure 4(e) and (f). For compound **2**, both the O3 and O4 hydroxyl groups could form intramolecular hydrogen bonds in both the quinoid and semiquinone radical structures, as shown in Figure 4(a) and (c), so the three rings in the molecule were coplanar. After the formation of the semiquinone radical, the bond length of the hydrogen bond was shortened from 0.1702 to 0.1608 nm, indicating that the hydrogen bond was strengthened after the formation of semiquinone radicals. Thus, compound **2** had a high EAE. However, for compound **4**, both in the quinoid structure and in the semiquinone radical structure, the O3 and O4 methoxyl groups did not form hydrogen bonds with O1 atoms but had a strong orbital repulsion, as shown in Figure 4(b) and (d). Moreover, this repulsion in the semiquinone radical structure was stronger than that in the quinoid structure because the electron cloud of the O1 anion/radical was more diffuse than that of the O1 atom of the carbonyl group, so the EAE of compound **4** was very small.

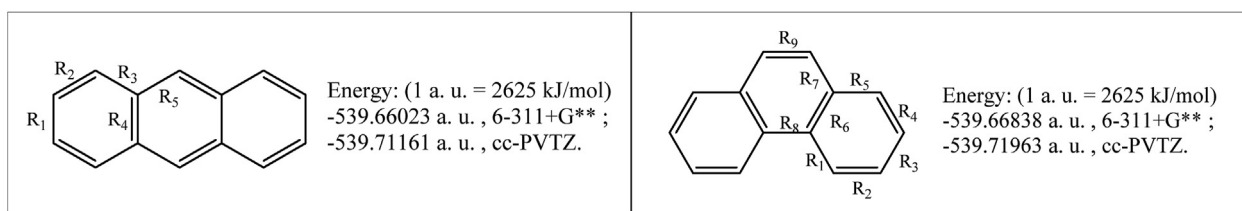


Figure 2. Definitions of bond lengths and calculated energies of anthracene (left) and phenanthrene (right).

Table 1. Calculated and observed bond lengths (0.1 nm) of anthracene and phenanthrene.

Anthracene	R <sub>1</sub>	R <sub>2</sub>	R <sub>3</sub>	R <sub>4</sub>	R <sub>5</sub>				
Ele. diff. (Ref. 19)	1.422	1.397	1.437	1.437	1.392				
X-ray (Ref. 20)	1.419	1.366	1.434	1.428	1.399				
6-311+G**	1.425	1.367	1.429	1.443	1.399				
cc-PVTZ	1.421	1.363	1.425	1.440	1.395				
cc-PVDZ (Ref. 21)	1.428	1.372	1.432	1.445	1.403				
Phenanthrene	R <sub>1</sub>	R <sub>2</sub>	R <sub>3</sub>	R <sub>4</sub>	R <sub>5</sub>	R <sub>6</sub>	R <sub>7</sub>	R <sub>8</sub>	R <sub>9</sub>
X-ray (Ref. 22)	1.405	1.383	1.391	1.381	1.457	1.404	1.395	1.448	1.372
6-311+G**	1.413	1.381	1.406	1.379	1.413	1.425	1.434	1.456	1.357
cc-PVTZ	1.410	1.377	1.402	1.375	1.409	1.421	1.431	1.453	1.353
cc-PVDZ (Ref. 21)	1.417	1.385	1.410	1.383	1.417	1.429	1.437	1.459	1.362

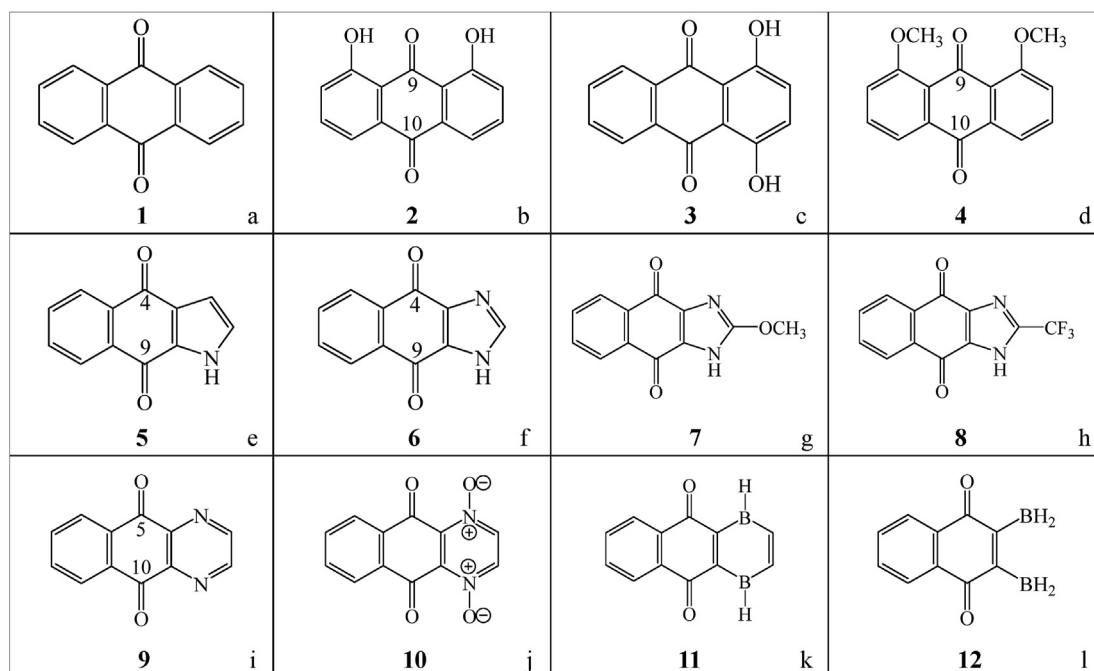


Figure 3. (a)–(l) Molecular structures and code numbers of polycyclic quinones calculated in this work.

Table 2. Calculated electron affinity energy (EAE) values for 12 polycyclic quinones.

Quinone	1	2	3	4	5	6
EAE (kJ/mol)	171.3	208.0	203.1	141.4	115.4	175.9
Quinone	7	8	9	10	11	12
EAE (kJ/mol)	169.6	210.7	197.4	224.6	275.0	239.5

### 3.2.2. Distributions of anion and radical

To compare the stability differences between resonance structures D and E, as well as between F and G, in Figure 4(e) and (f), the charges and spin densities of the O1 and O2 atoms in the semiquinone radical structures of compounds 2 and 4 were calculated. For compound 2, the results were O1 (−0.55, 0.16) and O2 (−0.36, 0.21), where the first values are charges, and the second are spin densities. This result indicated that the negative charge was mainly located on the O1 atom and the radical was mainly located on the O2 atom, which means that D was more stable than E. The reason for this was that the anion formed hydrogen bonds more easily than the radical. For compound 4, the result was O1 (−0.32, 0.20), O2 (−0.39, 0.24), C6/C8 (+0.48, 0.084), and C5/C9 (+0.073, 0.029). Since C6 and C8 atoms resonated with O1 atom while C5 and C9 atoms resonated with O2 atom, the negative charge was mainly located on the O2 atom and the radical was mainly located on the O1 atom, which means that G was more stable than F. The reason for this was that the repulsion of the radical was weaker than that of the anion.

To further reduce the repulsion in the G structure, the G structure resonated with two new resonance structures, J and K, as shown in Figure 4(g). The J and K structures both dispersed the radical of the O1 atom and reduced the orbital repulsion between the two methoxyl groups and the O1 atom. The evidence of the resonance is shown in Figure 4(d): the bond length of C7–O1 (0.1243 nm) was much shorter than that of C10–O2 (0.1261 nm), while the bond length of C7–C6 (0.1480 nm) was much longer than that of C5–C10 (0.1460 nm).

### 3.3. Polycyclic quinones containing five-membered heterocyclic ring

#### 3.3.1. Conjugation effect in the quinoid structure

Among the polycyclic quinones with imidazole rings (6–8), compounds 7 and 8 possessed the smallest and largest EAEs, respectively. The

optimized quinoid structure of compound 7 is shown in Figure 5(a), and its resonance structures are shown in Figure 5(b). As shown in Figure 5(a), the bond length of C11–O3 (0.1326 nm) was significantly shorter than that of C12–O3 (0.1444 nm), implying a strong conjugated effect of the methoxyl group with the imidazole ring. Since the N2 atom also had a lone pair of electrons, there was also a conjugation effect between the N2 atom and the C7–O1 group. These two conjugated effects are shown in Figure 5(b). Since the electron delocalized system of the M structure was larger than that of the N structure, the contribution of M was larger than that of N. The evidence of this conclusion was that the bond length of C7–O1 was shorter than that of C10–O2 and the bond length of C7–C8 was longer than that of C9–C10. This result indicated that the methoxyl group stabilized the quinoid structure of compound 7 because it was an electron-donating group. However, the trifluoromethyl group was not an electron-donating group, so the quinoid structure of compound 8 (Figure 5(e)) was not as stable as compound 7.

#### 3.3.2. Reliability verification of calculation results

The crystal structure of compound 8 was obtained in this work (CCDC code: 2130444). The crystal structure and optimized structure of compound 8 are shown in Figure 5(d), (e), respectively. The crystal data of compound 8 are shown in the supporting information.

As shown in Figure 5(d), (e), the bond lengths of the optimized structures were all generally close to those of the crystal structure, and the differences were all within 0.002 nm, except for those of CF<sub>3</sub>, indicating that the calculated results of this work were reliable.

#### 3.3.3. Inductive effect in semiquinone radical structure

The quinoid structures of compounds 7 (Figure 5(a)) and 8 (Figure 5(e)) were compared. The bond length of the C11–O3 of compound 7 in the semiquinone radical structure (Figure 5(c)) became longer (from 0.1326 to 0.1351 nm), but that of the C11–C12 of compound 8 in the semiquinone radical structure (Figure 5(f)) became shorter (from 0.1504 to 0.1490 nm), which indicated that the methoxyl group could not stabilize semiquinone radicals, while the trifluoromethyl group could stabilize the semiquinone radical well. Unlike the quinoid structure, the semiquinone radical structure was electron-rich, so the trifluoromethyl group could stabilize it well. This stabilizing action can be represented by the resonance structures of Figure 5(g). Figure 5(g) can be proven by the

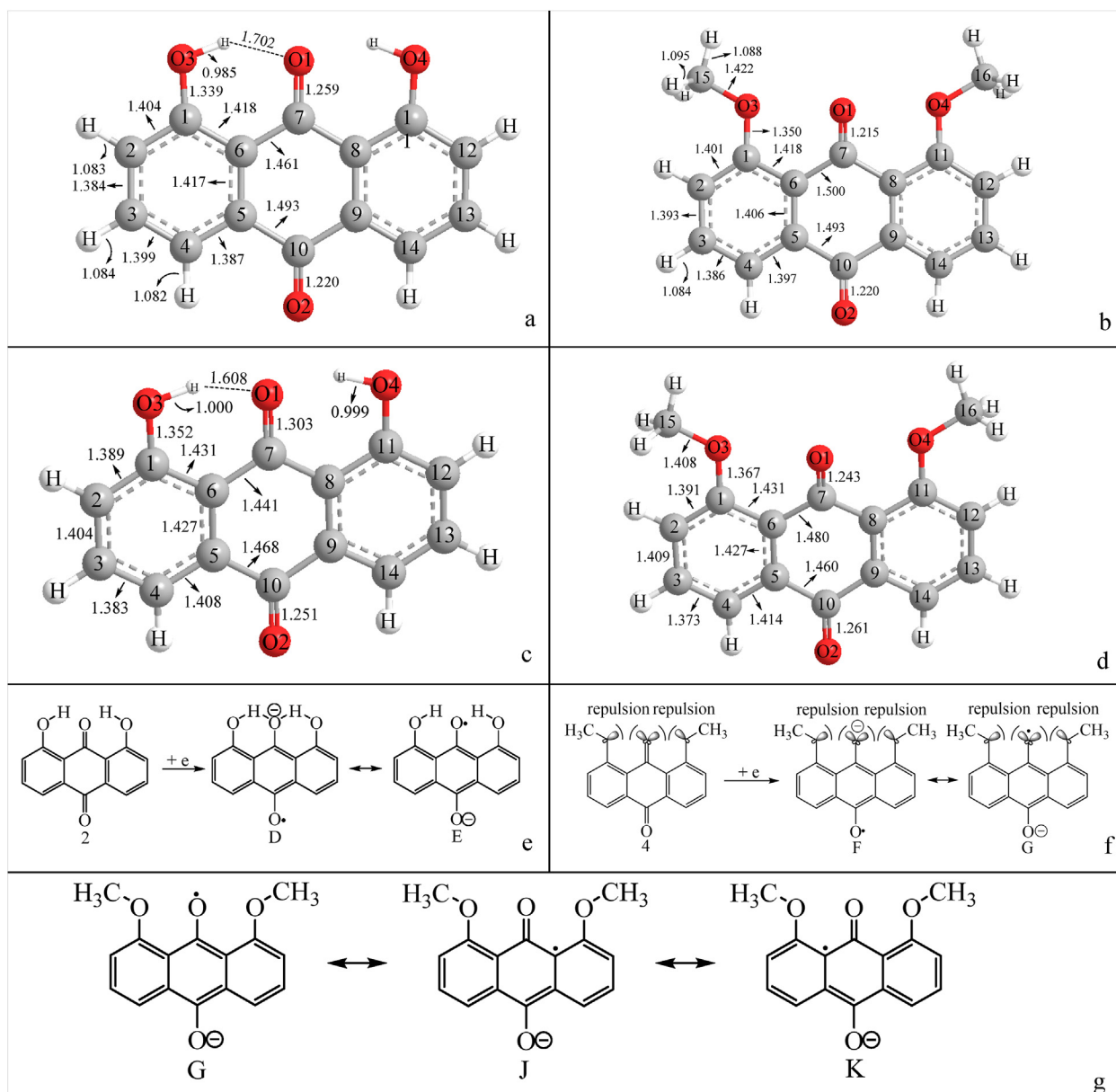


**Figure 4.** (a) Optimized quinoid structure of compound 2. Integers represent carbon atoms and their numbers, and decimals represent bond lengths in units of 0.1 nm. This notation is the same throughout the article. (b) Optimized quinoid structure of compound 4. (c) Optimized semiquinone radical structure of compound 2. (d) Optimized semiquinone radical structure of compound 4. (e) Resonance structures of the semiquinone radical of compound 2. (f) Resonance structures of the semiquinone radical of compounds 4. (g) Resonance structures of G structure.

information shown in Figure 5(f): the bond lengths of C7–O1 (0.1247 nm) and C8–N1 (0.1383 nm) in compound 8 were both shorter than the corresponding bond lengths in compound 7 (Figure 5(c), 0.1253 and 0.1400 nm). However, the bond lengths of C7–O8 (0.1450 nm) and N1–C11 (0.1308 nm) were both longer than the corresponding bond lengths in compound 7 (Figure 5(c), 0.1443 and 0.1301 nm).

In summary, the methoxyl group could stabilize the quinoid structure of compound 7 but not its semiquinone radical structure. The trifluoromethyl group could not stabilize the quinoid structure of compound 8, but it could stabilize its semiquinone radical structure. This was the reason that compound 8 had a much higher EAE than compound 7.

### 3.4. Polycyclic quinones containing six-membered heterocyclic rings

The optimized quinoid/semiquinone structures of compounds 9 and 10, as well as the resonance structures of the semiquinone radical structure of compound 10, are shown in Figure 6.

#### 3.4.1. Selection of conjugate direction

In the polycyclic quinones containing five-membered heterocyclic rings, carbonyl groups conjugated mainly with heterocyclic rings, both in the quinoid structures and semiquinone radical structures. However, this was not the case in polycyclic quinones containing six-membered heterocyclic rings. With compound 10 as an example, in the quinoid structure (Figure 6(b)), the bond length of C7–C6 was significantly shorter than that of C7–C8, but in the semiquinone radical structure (Figure 6(d)), the bond length of C7–C6 was significantly longer than that of C7–C8, indicating that the carbonyl groups conjugated mainly with the benzene ring in the quinoid structure and with the pyrazine ring in the semiquinone radical structure. The reason was that the carbonyl groups in the quinoid structure were electron-withdrawing groups, which preferentially conjugated with the benzene ring whose electron density was higher than that of the pyrazine ring. In the semiquinone radical structure, the carbonyl groups became an anion radical, which was electron-rich, so it conjugated with the pyrazine ring preferentially because the

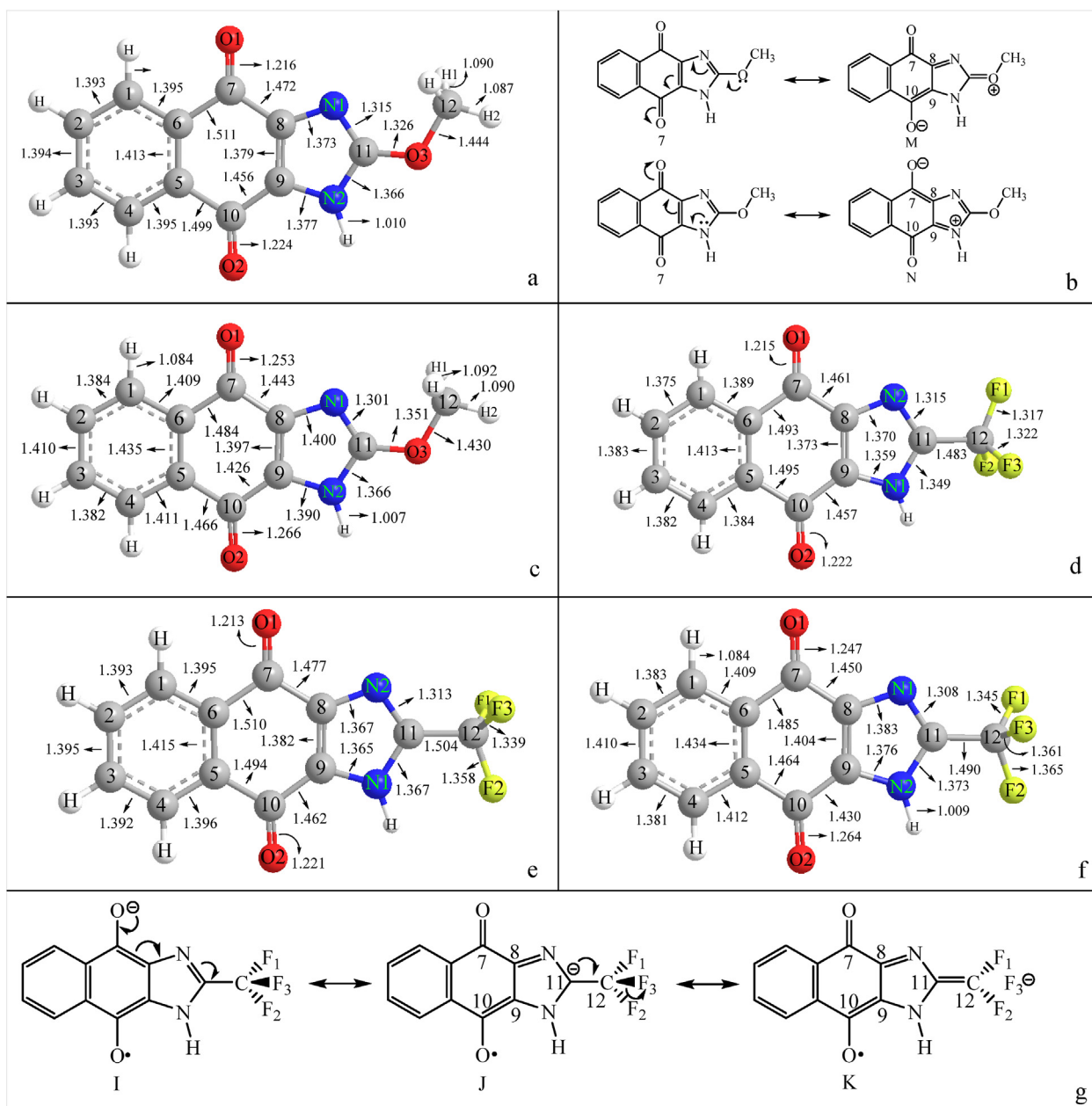


**Figure 5.** (a) Optimized quinoid structure of compound 7. (b) Resonant structures of quinoid structure of compound 7. (c) Optimized semiquinone radical structure of compound 7. (d) Crystal structure of compound 8. (e) Optimized quinoid structure of compound 8. (f) Optimized semiquinone radical structure of compound 8. (g) Resonant structures of the semiquinone radical of compound 8.

pyrazine ring had a stronger ability to attract electrons than the benzene ring.

In the quinoid structure of compound 10, the charge distribution of the benzene ring was such that C1 and C4 both had charges of +0.34, C2 and C3 both had charges of -0.16, and C5 and C6 both had charges of +0.41. It is predicted that the carbonyl groups mainly conjugated with C5 and C6 atoms. The 48<sup>th</sup> molecular orbital of the quinoid structure of compound 10 was calculated, which is shown in Figure 7(a). This molecular orbital proved that the two carbonyls together with C5 and C6 atoms formed a local conjugate system that contained six centers and six electrons. The lowest unoccupied molecular orbital (LUMO) of the local conjugate system is shown in Figure 7(b). In the semiquinone radical structure of compound 10, the LUMO should be occupied. Since C7 and C6, as well as C5 and C10, bonded in the LUMO, the bond lengths of C7-C6 and C5-C10 in the semiquinone radical structure were both shorter than those in the quinoid structure.

### 3.4.2. Repulsion disappeared

Compound 9 was a planar molecule in both the quinoid structure and the semiquinone radical structure, so it had no spatial repulsion. However, compound 10 was not a planar molecule in the quinoid structure, and the dihedral angle O1-C7-N2-O3 was 11.7°, as shown in Figure 6(e), because the p orbitals of the O1 and O3 atoms repelled each other. The distance between the two O atoms was 0.2620 nm, slightly less than twice the van der Waals radius (0.1400 nm). In the semiquinone radical structure of compound 10 (Figure 6(f)), the dihedral angle O1-C7-N2-O3 was only 0.3°, and the entire molecule was almost coplanar, implying that the spatial repulsion existing in the quinoid structure disappeared, which was one reason that the EAE of compound 10 was higher than that of compound 9. It remains to be answered why the spatial repulsion disappeared in the semiquinone radical structure of compound 10.

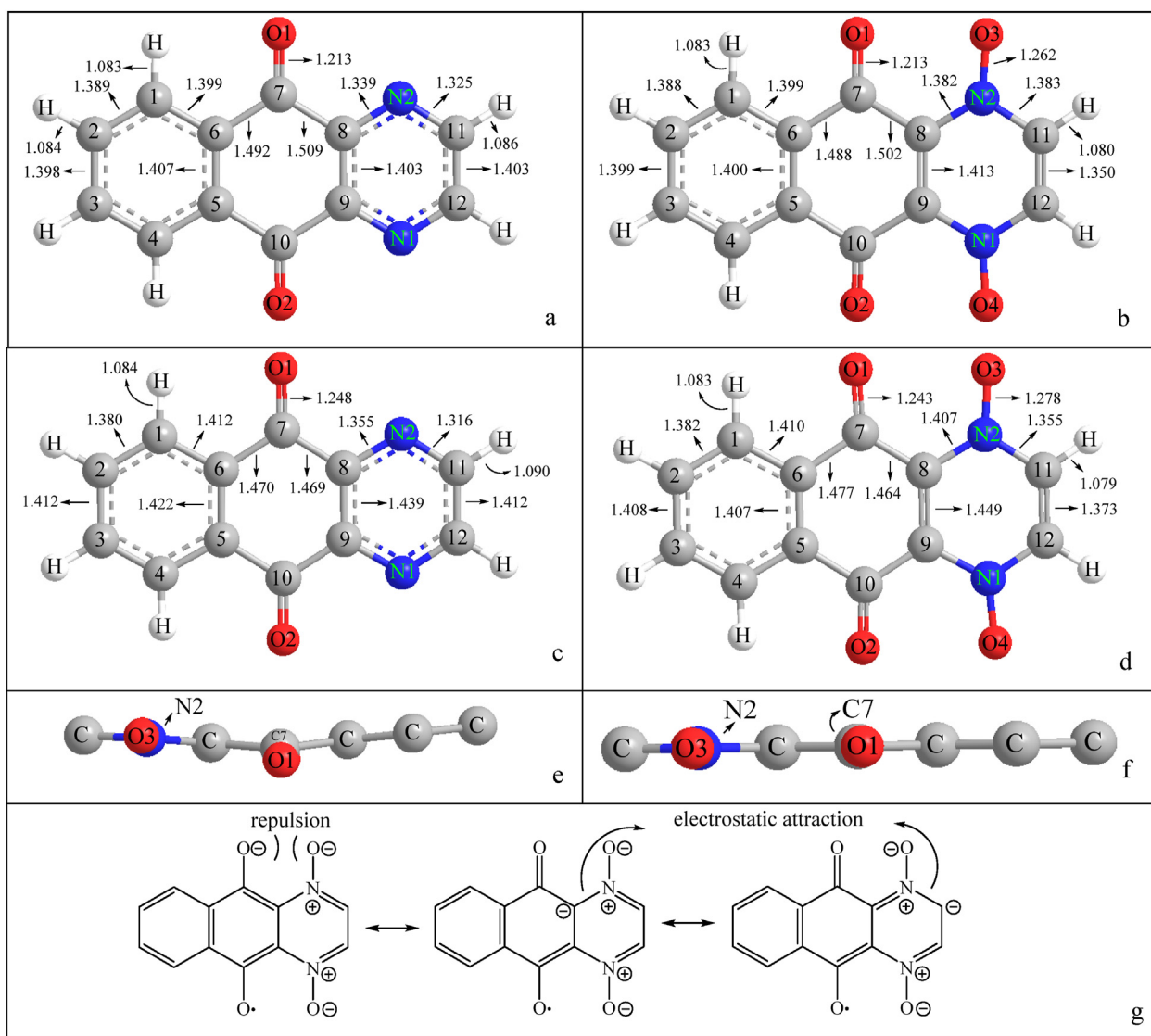


**Figure 6.** (a) Optimized quinoid structure of compound 9. (b) Optimized quinoid structure of compound 10. (c) Optimized semiquinone radical structure of compound 10. (d) Optimized semiquinone radical structure of compound 10. (e) Side view of the optimized quinoid structure of compound 10 (H atoms omitted). (f) Side view of the optimized semiquinone radical structure of compound 10 (H atoms omitted). (g) Electrostatic action in the resonant structures of the optimized semiquinone radical structure of compound 10.

### 3.4.3. Electrostatic interactions

The highest occupied molecular orbitals (HOMOs) of the semiquinone radical structures of compounds 9 and 10 were calculated. The results are shown in Figure 7(c), (d). The HOMO of the semiquinone radical structure of polycyclic quinone was occupied by a single electron. Typically, a single electron occupies the antibonding orbital of the  $\pi$  bonds of carbonyl groups, so the bond lengths of C–O bonds in semiquinone radical structures are longer than those in quinoid structures. If

the single electron can disperse to many other orbitals, the semiquinone radical will be stabilized. As shown in Figure 7(c), the electron dispersion effect of the HOMO of compound 10 was significantly better than that of compound 9 (Figure 7(d)), which was another reason that the EAE of compound 10 was higher than that of compound 9.

For convenience, in this paper, the differences in the values of the electron population of an atom (or group) between the semiquinone radical structure and quinoid structure are called the added value. For

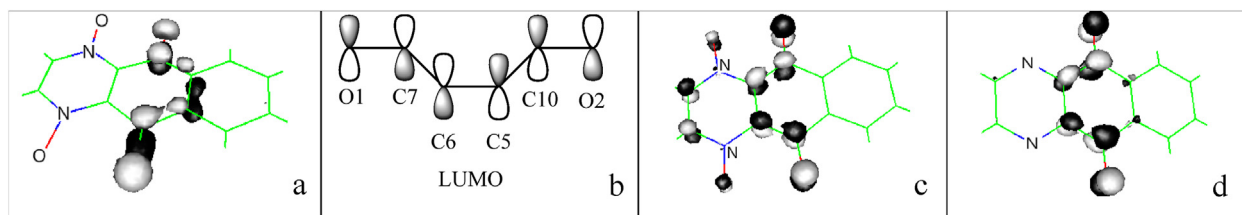


**Figure 7.** (a) Forty-eighth molecular orbital of quinoid structure of compound 10. (b) Lowest unoccupied molecular orbital (LUMO) of the local conjugate system. (c) Highest occupied molecular orbital (HOMO) of semiquinone radical structure of compound 10. (d) HOMO of semiquinone radical structure of compound 9.

compound **10**, the added value of the benzene ring was +0.45, that of two carbonyl groups was -0.53, and that of pyrazine-oxide ring was +1.08, which indicated that the single electron of the semiquinone radical of compound **10** almost dispersed in the pyrazine-oxide ring and not in the two carbonyl groups. In the pyrazine-oxide ring, the added values of the C8 and C9 atoms were both +0.33, and they were the most important contributor to the added value. The reason that a single electron preferentially dispersed on C8 and C9 atoms and not on the carbonyl groups was that such an electronic distribution had the following three advantages: (1) if the values of the electron population of O atoms of the carbonyl groups increased, the spatial repulsion between the O3/O4 atoms and carbonyl groups would increase. (2) The negative charges of C8 and C9 could form electrostatic interactions with the positive charges of the N2 and N1 atoms. (3) The electrons of C8 or C9 could be delocalized to the C11 and C12 atoms by resonance. These advantages are depicted in Figure 6(g).

In compound **9**, the N atoms did not carry a positive charge, and there were no O3 and O4 atoms that generated spatial repulsion with the carbonyl groups, so the resonance shown in Figure 6(g) was absent in its semiquinone radical structure. The added values of C8 and C9 atoms both were only +0.02, but those of the carbonyl groups were both +0.24, indicating that the negative charge and radical of the semiquinone radical of compound **9** were mainly dispersed on the O atoms.

Figure 6(g) shows the semiquinone radical structure of compound **10**. The carbonyl groups had a strong conjugation effect with the pyrazine-oxide ring, dispersing the excess electrons, which caused the whole molecule to be coplanar. In its quinoid structure, this conjugated effect did not exist, so the spatial exclusion was dominant, which led to a nonplanar structure.

### 3.5. Polycyclic quinones containing B atoms

The quinoid structures and the semiquinone radical structures of compounds **11** and **12** are shown in Figure 8.

#### 3.5.1. Effect of antiaromaticity on structure

A unique feature in the quinoid structure of compound **11** was that its six-membered ring containing two boron atoms was not planar, where the dihedral angle H1-B2-C12-H2 was 22.1°. This structure was similar to the boat conformation of cyclohexane, with the two boron atoms located in the two bow positions, as shown in Figure 8(a). The nonplanar structure of this six-membered ring was not due to spatial repulsion, as shown in the quinoid structure of compound **10**, because there were no atoms to produce the repulsion. If the six-membered ring adopted a coplanar structure, its  $\pi$  system would contain four  $\pi$  electrons (coming from two  $\pi$  bonds), which should be antiaromatic. Since antiaromaticity was absent in the semiquinone radical structure of compound **11**, it was coplanar, as shown in Figure 8(b).

#### 3.5.2. Orbital interaction

Compound **11** had the largest EAE in this paper, implying that its semiquinone radical structure was very stable. To understand the reason, the HOMO of the semiquinone radical of compound **11** was calculated, which is shown in Figure 9 (left).

Figure 9 (left) shows that the single electron in the HOMO was dispersed mainly in  $\pi$  bonds of C8-B1 and C9-B2. Figure 9 (right) shows how the two bonds were generated based on valence bond theory. Anions and radicals on the O1 and O2 atoms could resonate with the C8 and C9 atoms and interact with the empty orbitals of adjacent B atoms to form a

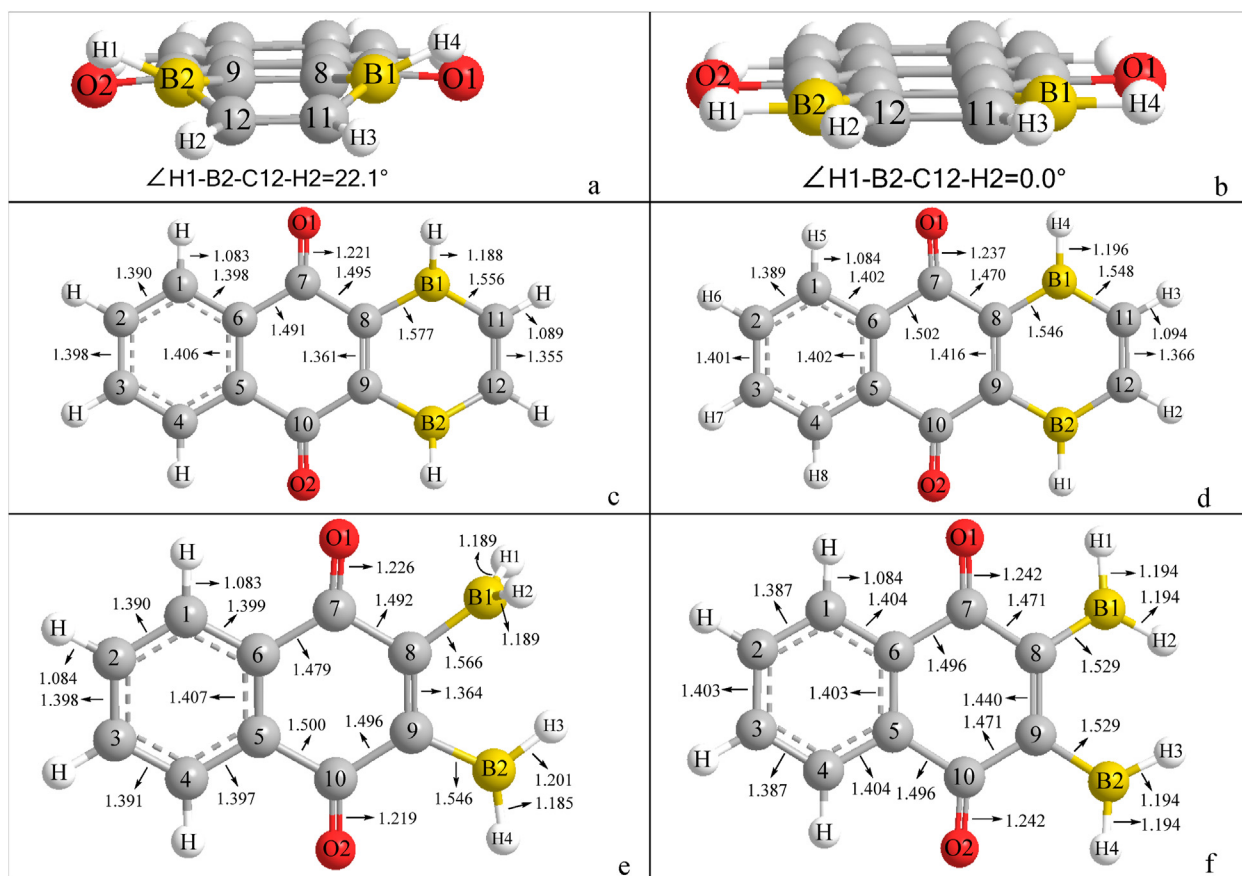


**Figure 8.** (a) Side view of the optimized quinoid structure of compound **11**. (b) Side view of the optimized semiquinone radical structure of compound **11**. (c) Top view of the optimized quinoid structure of compound **11**. (d) Top view of the optimized semiquinone radical structure of compound **11**. (e) Top view of the optimized quinoid structure of compound **12**. (f) Top view of the optimized semiquinone radical structure of compound **12**.

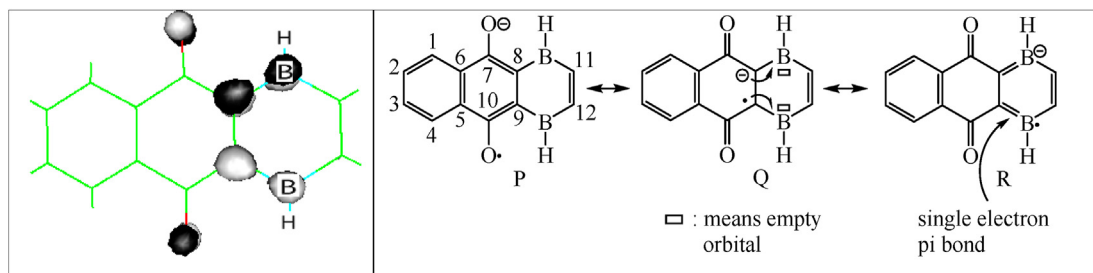


**Figure 9.** HOMO of the semiquinone radical structure of compound 11 (left) and the valence bond theoretical depiction of this structure (right).

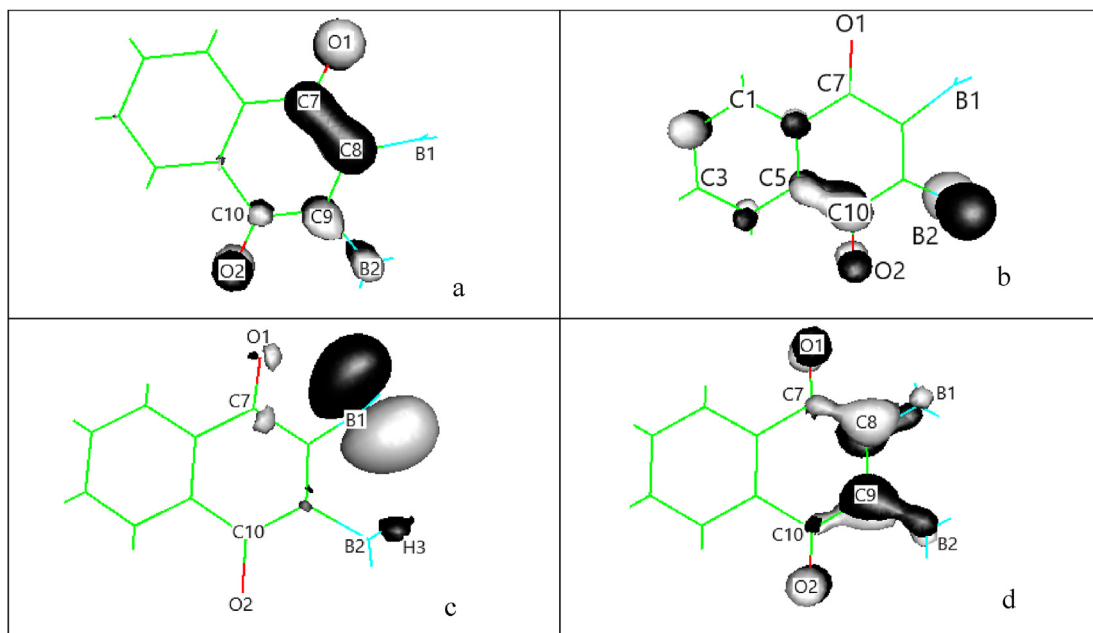


**Figure 10.** (a) LUMO (48th molecular orbital) of quinoid structure of compound 12. (b) LUMO+1 (49<sup>th</sup> MO) of quinoid structure of compound 12. (c) LUMO+2 (50<sup>th</sup> MO) of quinoid structure of compound 12. (d) HOMO (48<sup>th</sup> MO) of semiquinone radical structure of compound 12.

two-electron  $\pi$  bond and a single-electron  $\pi$  bond, respectively, making the anion and radical stable. This orbital interaction was supported by the analysis of the electron population. The added value of the two carbonyl groups was  $-0.16$ , and those of the benzene ring and six-membered ring containing B atoms were  $+0.44$  and  $+0.72$ , respectively, which indicated the single electron dispersed mainly on the six-membered ring containing B atoms. In the semiquinone structure of compound 11, the spin densities of C8, C9, and the two B atoms were all approximately 0.20, while those of O1 and O2 were both only 0.12 (the sum of the other atoms was  $-0.04$ ), indicating that the radical dispersed mainly on B atoms, not O atoms. That is, the contribution of the Q and R structures was greater than that of the P structure. Finally, the C–O bond length in the semiquinone radical structure of compound 11 was only 0.1237 nm, the shortest of all the semiquinone radical structures, which was consistent with the fact that the P structure had a small contribution.

The quinoid structure of compound 12 (Figure 8(e)) is called 2,3-diboranyl-1,4-naphthoquinone. Its two  $\text{BH}_2$  groups are chemically inequivalent, with the one (B2H3H4 group) coplanar to the plane of naphthoquinone and the other (B1H1H2 group) perpendicular to it. For the quinoid structure of compound 12, the LUMO was an antibonding orbital of delocalized large  $\pi$  bonds, which consisted of O1, C7, C8, C9, C10, and O2 atoms, as shown in Figure 10(a). The empty orbitals of the B2 and B1 atoms were the main component of LUMO+1 (49<sup>th</sup> orbital) and LUMO+2 (50<sup>th</sup> orbital), respectively, as shown in Figures 10(b) and 10(c). As shown in Figure 10(b), the empty orbital of the B2 atom interacted with the C5–C10  $\pi$  bonding orbital and C10–O2  $\pi$  antibonding orbital, so the

bond levels of the C5–C10  $\pi$  bond were weakened and those of the C10–O2  $\pi$  bond were strengthened. This was the reason that the bond length of C5–C10 (0.1500 nm) was much greater than that of C6–C7 (0.1479 nm), and the bond length of C10–O2 (0.1219 nm) was less than that of C7–O1 (0.1226 nm). As shown in Figure 10(c), there was a weak interaction between the H3 atom and the empty orbital of the B1 atom. It is possible that the H3 atom donated its 1s electron to the empty orbital of the B1 atom, so the bond length of B2–H3 (0.1201 nm) was longer than that of B2–H4 (0.1185 nm).

In the semiquinone radical structure of compound 12, the two  $\text{BH}_2$  groups were chemically equivalent, and they both were approximately coplanar to the plane of naphthoquinone, as shown in Figure 10(d). Figure 10(d) shows the HOMO of the semiquinone radical structure of compound 12. The single electron of the HOMO dispersed mainly on the  $\pi$  orbitals of the C8 and C9 atoms but not of the O1 and O2 atoms. The  $\pi$  orbitals of the C8 and C9 atoms both interacted with the empty orbitals of the B atoms, indicating that the empty orbitals of the B atoms could stabilize the semiquinone radical structure. Thus, compound 12 possessed a large EAE of 239.5 kJ/mol.

#### 4. Conclusions

The EAEs of polycyclic quinones depend on the energy difference between the quinoid structures and the semiquinone radical structures. For compound 2, there were hydrogen bonds in both the quinoid structure and semiquinone radical structure, and the hydrogen bond in the semiquinone

radical structure was stronger than that in the quinoid structure. Thus, compound 2 had a large EAE. For compound 4, there was spatial repulsion in both the quinoid structure and semiquinone radical structure, and the spatial repulsion in the semiquinone radical structure was larger than that in the quinoid structure. Thus, compound 4 had a small EAE. For compound 5, the electron-donating group (OCH<sub>3</sub>) stabilized the quinoid structure but not the semiquinone radical structure by the conjugative effect, while for compound 7, the electron-withdrawing group (CF<sub>3</sub>) stabilized the semiquinone radical structure and not the quinoid structure. Thus, the EAE of compound 7 was larger than that of compound 5. The spatial repulsion made the quinoid structure of compound 10 less stable than compound 9, but the positive charge of compound 10 provided electrostatic interactions to stabilize the semiquinone radical structure. Since there were no such electrostatic interactions in the semiquinone radical structure of compound 9, its EAE was less than that of compound 10. The quinoid structure of compound 11 was antiaromatic, but its semiquinone radical structure was not. Moreover, boron atoms of compound 11 could provide empty orbitals to stabilize semiquinone radical anions by orbital interactions. Since compound 11 had a very unstable quinoid structure and a very stable semiquinone radical structure, it had the largest EAE of all the compounds studied in this work.

This was a theoretical study on the relationship between the EAE and the molecular structure. Whether the research results are correct still requires the verification of experimental results. Since the EAE is closely related to ROSs and anticancer activity, this work will provide a reference for pharmaceutical chemists to design anticancer drugs at the molecular level.

## Declarations

### Author contribution statement

Xucheng Wang: Performed the experiments; Analyzed and interpreted the data; Wrote the paper.

Yao Cheng: Performed the experiments; Analyzed and interpreted the data.

Yaofeng Yuan, Yongfan Zhang: Contributed reagents, materials, analysis tools or data.

Wenfeng Wang: Conceived and designed the experiments; Wrote the paper.

### Funding statement

This work was supported by National Natural Science Foundation of China (22071025 & 21772023).

### Data availability statement

Data included in article/supplementary material/referenced in article.

### Declaration of interests statement

The authors declare no conflict of interest.

### Additional information

No additional information is available for this paper.

## References

- [1] S. Pan, Y. Zhou, Q. Wang, Y. Wang, C. Tian, T. Wang, L. Huang, J. Nan, L. Li, S. Yang, Discovery and structure-activity relationship studies of 1-aryl-1*H*-naphtho[2,3-*d*][1,2,3]triazole-4,9-dione derivatives as potent dual inhibitors of indoleamine 2,3-dioxygenase 1 (Ido1) and tryptophan 2,3-dioxygenase (TDO), *Eur. J. Med. Chem.* 207 (2020), 112703.
- [2] L. Zhang, G. Zhang, S. Xu, Y. Song, Recent advances of quinones as a privileged structure in drug discovery, *Eur. J. Med. Chem.* 223 (2021), 113632.
- [3] X.W. Xie, Z.P. Liu, X. Li, Design, synthesis, bioevaluation of LFC- and PA-tethered anthraquinone analogues of mitoxantrone, *Bioorg. Chem.* 101 (2020), 104005.
- [4] J.S. Al-Otaibi, T.M.E.L. Gogary, Synthesis of novel anthraquinones: molecular structure, molecular chemical reactivity descriptors and interactions with DNA as antibiotic and anti-cancer drugs, *J. Mol. Struct.* 1130 (2017) 799–809.
- [5] S.S. Pan, L. Pedersen, N.R. Bachur, Comparative flavoprotein catalysis of anthracycline antibiotic—reductive cleavage and oxygen-consumption, *Mol. Pharmacol.* 19 (1981) 184–186.
- [6] R.P. Hertzberg, P.B. Dervan, Cleavage of DNA with methidiumpropyl-EDTA-iron(II): reaction conditions and product analyses, *Biochem. J.* 23 (1984) 3934–3945.
- [7] A.G.G. Tonolo, C. Curti, T. Terme, P. Vanelle, A survey of synthetic routes and antitumor activities for benzo[*g*]quinoxaline-5,10-diones, *Molecules* 25 (2020) 5922.
- [8] H. Lee, S. Cho, K. Namgoong, J.K. Jung, J. Chob, S.I. Yang, Synthesis and in vitro evaluation of 7-dialkylaminomethylbenzo[*g*]quinoxaline-5,10-diones, *Bioorg. Med. Chem. Lett.* 14 (2004) 1235–1237.
- [9] Z. Liu, Z. Zhang, W. Zhang, D. Yan, 2-Substituted-1-(2-morpholinoethyl)-1*H*-naphtho[2,3-*d*]imidazole-4,9-diones: design, synthesis and antiproliferative activity, *Bioorg. Med. Chem. Lett.* 28 (2018) 2454–2458.
- [10] S.H.S. Ho, M.Y. Sim, W.L.S. Yee, T. Yang, S.P.J. Yuen, M.L. Go, Antiproliferative, DNA intercalation and redox cycling activities of dioxonaphtho[2,3-*d*]imidazolium analogs of YM155: a structure-activity relationship study, *Eur. J. Med. Chem.* 104 (2015) 42–56.
- [11] Q. Zhou, C. Peng, F. Du, L. Zhou, Y. Shi, Y. Du, D. Liu, W. Sun, M. Zhang, G. Chen, Design, synthesis and activity of BBI608 derivatives targeting on stem cells, *Eur. J. Med. Chem.* 151 (2018) 39–50.
- [12] Y. Subramaniam, K. Subban, J. Chellia, A novel synergistic anticancer effect of fungal cholestanol glucoside and paclitaxel: apoptosis induced by an intrinsic pathway through ROS generation in cervical cancer cell line (HeLa), *Toxicol. Vitro* 72 (2021), 105079.
- [13] J. Qian, Z. Xu, C. Meng, J. Liu, P.L. Hsu, Y. Li, W. Zhu, Y. Yang, S.L.M. Natschke, K.H. Lee, Y. Zhang, Y. Ling, Design and synthesis of benzylidenecyclohexenones as TrxR inhibitors displaying high anticancer activity and inducing ROS, apoptosis, and autophagy, *Eur. J. Med. Chem.* 204 (2020), 112610.
- [14] S.M. Cheng, T.Y. Lin, Y.C. Chang, I.W. Lin, E. Leung, C.H.A. Cheung, YM155 and BIRC5 downregulation induce genomic instability via autophagy-mediated ROS production and inhibition in DNA repair, *Pharm. Res. (N. Y.)* 166 (2021), 10547.
- [15] Z. Zuo, X. Liu, X. Qian, T. Zeng, N. Sang, H. Liu, Y. Zhou, L. Tao, X. Zhou, N. Su, Y. Yu, Q. Chen, Y. Luo, Y. Zhao, Bifunctional naphtho[2,3-*d*][1,2,3]triazole-4,9-dione compounds exhibit antitumor effects in vitro and in vivo by inhibiting dihydroorotate dehydrogenase and inducing reactive oxygen species production, *J. Med. Chem.* 63 (2020) 7633–7652.
- [16] Y. Zheng, L. Zhu, L. Fan, W. Zhao, J. Wang, X. Hao, Y. Zhu, X. Hu, Y. Yuan, J. Shao, W. Wang, Synthesis, SAR and pharmacological characterization of novel anthraquinone cation compounds as potential anticancer agents, *Eur. J. Med. Chem.* 125 (2017) 902–913.
- [17] J.P. Anzenbacher, M.A. Palacios, K. Jursikova, M. Marquez, Simple electrooptical sensors for inorganic anions, *Org. Lett.* 7 (2005) 5027–5030.
- [18] Z.X. Liu, Z.F. Zhang, W.B. Zhang, D.Y. Yan, 2-Substituted-1-(2-morpholinoethyl)-1*H*-naphtho[2,3-*d*]imidazole-4,9-diones: design, synthesis and antiproliferative activity, *Bioorg. Med. Chem. Lett.* 28 (2018) 2454–2458.
- [19] S.N. Ketker, M. Kelley, M. Fink, R.C. Ivey, On an electron diffraction study of the structures of anthraquinone and anthracene, *J. Mol. Struct.* 77 (1981) 127–138.
- [20] Q. Xing, W. Pei, R. Xu, J. Pei, *Basic Organic Chemistry (II)*, fourth ed., Peking University Press, China, 2017, p. p719 (In Chinese).
- [21] J.M.L. Martin, J. El-Yazal, J.P. François, Structure and vibrational spectrum of some polycyclic aromatic compounds studied by density functional theory. 1. Naphthalene, azulene, phenanthrene, and anthracene, *J. Phys. Chem.* 100 (1996) 15358–15367.
- [22] J. Trotter, The crystal and molecular structure of phenanthrene, *Acta Crystallogr.* 16 (1963) 605–608.
- [23] R.D. Hancock, I.V. Likolayenko, Do nonbonded H–H interactions in phenanthrene stabilize it relative to anthracene? A possible resolution to this question and its implications for ligands such as 2,2'-Bipyridyl, *J. Phys. Chem. A* 116 (2012) 8572–8583.